JOURNAL OF MATERIALS SCIENCE 33 (1998) 803–809

Mechanical behaviour of metal–matrix composite deposits

X. M. DING, N. MERK, B. ILSCHNER
Mechanical Metallurgy Laboratory, Materials Science Department, Federal Institute of Technology, 1015 Lausanne, Switzerland

The electroplating technique is used for producing thin sheets of copper- or nickel-based composites containing different volume fractions of α-alumina dispersions. The microhardness and tensile behaviour of such composites, in both the as-deposited and the annealed state, are characterized. The strengthening mechanism of electroplated composites is found to be a combination of Orowan-type strengthening and the Hall–Petch effect. © *1998 Chapman & Hall*

1. Introduction

Producing composite thin sheets by electrodeposition is an inexpensive process which can be performed near room temperature [1–5]. Since the deposition current density affects directly the amount of codeposited particles [6, 7], it can be used to prepare composite deposits of different particle volume fractions [8]. Superior wear resistance, microhardness and strength compared with the corresponding values for pure metal or alloy deposits are characteristic features of composite deposits [1, 9–12]. Cu–alumina [13, 14] or Ni–alumina [15, 16] composite coatings exhibit higher yield and ultimate tensile strengths and lower ductilities than pure copper or nickel deposits, maintaining these characteristics even after annealing. A hardening mechanism which has received much attention is the Orowan mechanism [15, 17]. However, this alone cannot explain the total strengthening which occurrs in composite deposits, especially those containing particles greater than 1 μm [8, 18]. Microstructural investigations have shown a high matrix defect density and a particle-induced grain refinement in the as-deposited state [8, 19]. This suggests that grain-boundary strengthening may be another mechanism to be taken into account.

We performed a series of microhardness and tensile tests on pure metal and on composite deposits in order to examine the modification of the mechanical properties of composites which are introduced by the codeposited particles. Tests have been equally carried out on annealed specimens, aiming to reveal the effect of heat treatment on their mechanical behaviour. Using structural parameters such as the matrix grain size, particle size and particle volume fraction for both as-deposited and annealed specimens, we present a detailed analysis of composite strengthening in such a way that the contribution of dispersion hardening (Orowan) and grain-boundary hardening (Hall–Petch) can be separated.

2. Experimental procedure

The metallic matrix was either copper or nickel metals. α-alumina with different average sizes of 2.7 μm (AOL), 0.4 μm (AOM) and 0.11 μm (AOS) were used. The deposition techniques and parameters have been presented elsewhere [8]. Tensile specimens of 70 μm thickness (Fig. 1a) were directly deposited on stainless steel cathodes having a central part with the exact shape of a tensile specimen. In this way, no further machining of the deposits was necessary, preventing the possible introduction of additional stress at the edges of the calibrating length. The purpose of keeping the surrounding part of the cathode is to obtain a homogeneous distribution of the deposition current over the tensile specimen. The constant thickness through the specimen and the good quality of specimen edges were controlled by scanning electron microscopy (SEM). Heat treatments at different temperatures were carried out for 1.0 h in a 5×10^{-4} mbar vacuum, using a HE 50/15 Pyrox furnace. Nickel blocks of 2 mm thickness were plated to the two ends of the tensile specimen which was then introduced into the two aligned grips of a clampless fixation system for the tensile testing of thin deposits (Fig. 1b). Tensile tests were performed using a commercial Zwick 1484 tensile-testing machine and the load was measured with a force sensor up to 500 N. *In-situ* measurement of deformation was carried out using a high-resolution video camera focused on two black marks located at each end of the calibrating length. Microhardness measurements were performed using a Leitz RZD-D0 digital microhardness device on the cross-section of deposits encircled by an electrodeposited nickel layer 200 μm thick. Because of the difficulty in determining the exact yield point on the tensile curves, the 0.2% proof stress has been taken as the yield stress. The reported values are the average results of three or more measurements.

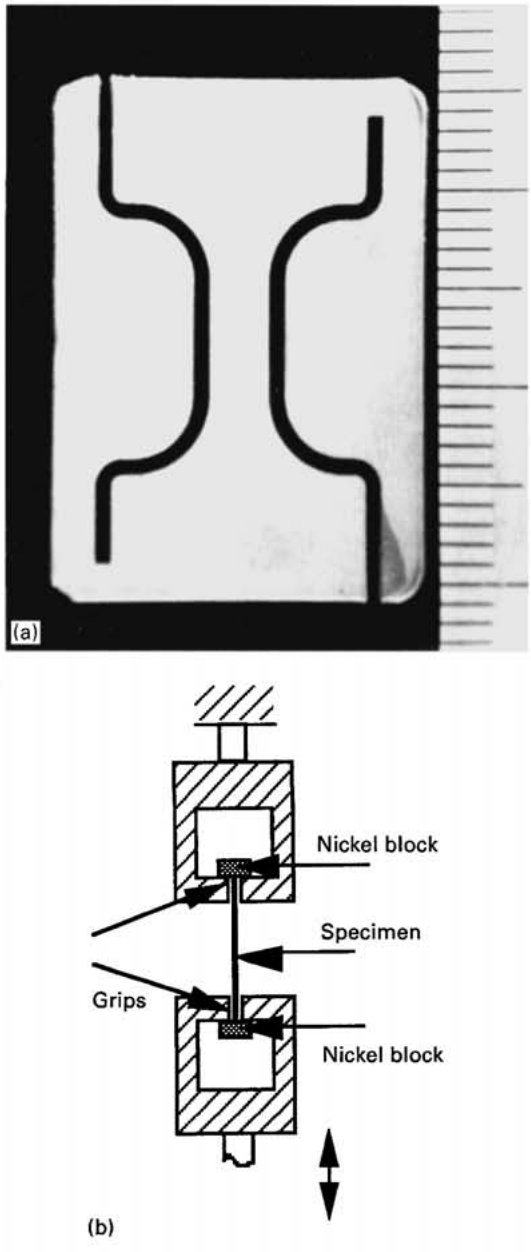

Figure 1 (a) A tensile specimen; (b) clampless fixation method.

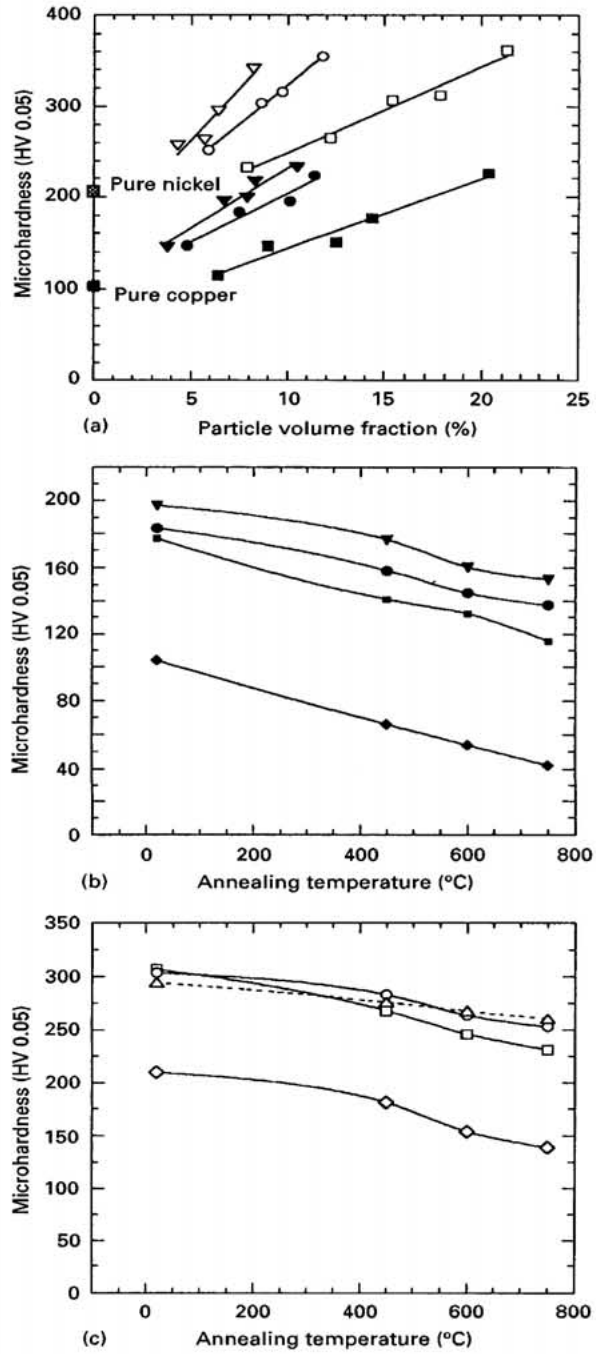

Figure 2 Microhardness of (a) as-deposited metal–alumina composites versus particle volume fraction ((▽), Ni–AOS; (○), Ni–AOM; (□), Ni–AOL; (▼), Cu–AOS; (●), Cu–AOM; (■), Cu–AOL) (b) annealed copper–alumina deposits versus annealing temperature ((◆), pure Cu; (■), Cu–AOL; (●), Cu–AOM; (▼), Cu–AOL)) and (c) nickel–alumina deposits versus annealing temperature ((◇), pure Ni; (□), Ni–AOL; (○), Ni–AOM; (△), Ni–AOS). The particle volume fractions are as follows: Cu–AOL, 14%; Cu–AOM, 8%; Cu–AOS, 7%; Ni–AOL, 15%; Ni–AOM, 9%; Ni–AOS, 6%.

3. Results

3.1. Microhardness

A linear increase in microhardness of metal–alumina composite specimens with particle volume fraction was observed. As shown in Fig. 2a, in comparison with particle-free deposits, a significant microhardness improvement is achieved by introducing second-phase particles. This is in agreement with other obtained results [13, 20]. Furthermore, a stronger hardening effect of submicron particles is observed in comparison with larger particles. The microhardnesses of annealed copper-based and nickel-based specimens are presented in Fig. 2b and c, respectively. A decrease in microhardness is observed for all the samples. The relative decrease compared with the as-deposited state is summarized in Table I, showing that the composite deposits exhibit a much better retention in hardness than the pure deposits. After annealing for 1 h at 750 °C, pure nickel specimens lose one third of their hardness while Ni–9% AOM specimens undergo a hardness drop of only 17%. It can be seen that a better retention in microhardness is obtained for smaller particles.

3.2. Tensile behaviour

Typical stress–strain curves of pure copper and nickel deposits, in the as-deposited and the annealed states, are presented in Fig. 3. Table II gives the measured strength and elongation of these deposits, together with the properties of massive copper and nickel at

TABLE I Relative decreases in Vickers microhardnesses of annealed deposits

Annealing temperature (°C)	Relative decrease in microhardness, $(\Delta HV/HV_0) \times 100$ (%)							
	Pure Cu	Cu–AOS	Cu–AOM	Cu–AOL	Pure Ni	Ni–AOS	Ni AOM	Ni–AOL
450	−37	−11	−14	−20	−14	− 6	− 7	−13
600	−46	−19	−21	−25	−27	−10	−13	−20
750	−59	−22	−25	−35	−34	−16	−17	−25

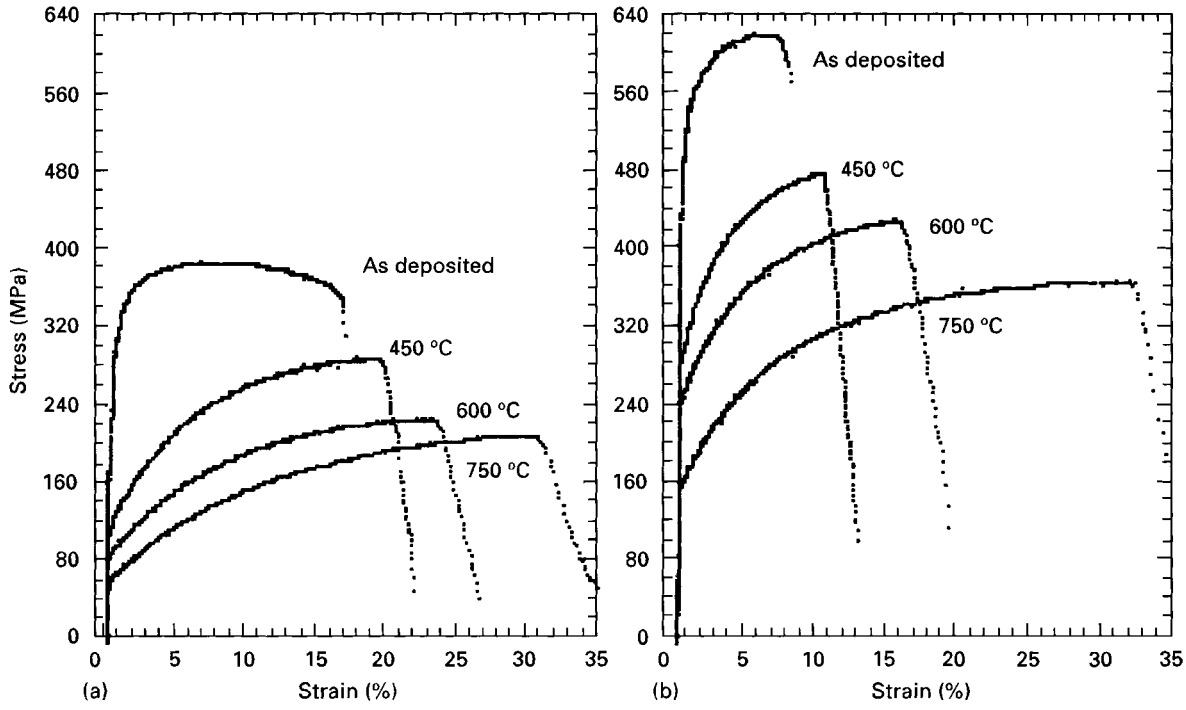

Figure 3 Stress–strain curves of (a) pure copper and (b) pure nickel deposits.

TABLE II Mechanical properties of pure copper and pure nickel deposits and massive copper and nickel

Material	Annealing temperature (°C)	0.2% yield stress (MPa)		Ultimate stress (MPa)		Elongation (%)	
		Cu	Ni	Cu	Ni	Cu	Ni
Deposit	As deposited	149	255	395	634	16.8	10.5
Deposit	450	113	196	296	490	20.1	14.1
Deposit	600	86	162	229	458	23.7	19.2
Deposit	750	66	113	218	376	30.2	32.0
Massive material	20	62	148	170	462	35	40

room temperature [21]. As can be seen, the electrodeposited samples with a grain size of about 1.0–2.0 μm [8] exhibit greater ultimate and yield strengths but less elongation than their massive counterparts with the grain size usually larger than 10.0 μm [21]. After annealing, a marked decrease in strength accompanied by an important increase in ductility is observed. The stress–strain curves of Cu–AOM and Ni–AOM deposits are presented in Fig. 4 and the corresponding measured properties are listed in Table III. Compared with the particle-free deposits, as-deposited composite specimens exhibit higher strength but a considerably reduced ductility. For example, Ni–9%AOM deposits show a 45% increase in yield strength and 17% in ultimate strength while undergoing a drastic loss in ductility of 73%. After heat treatment, composite deposits show good retention of both yield and ultimate strength, together with a marked improvement in ductility. Further, in comparison with the annealed metal deposits, the annealed composite deposits show much less strain hardening.

The yield strength of as-deposited composite samples is plotted in Fig. 5a versus the particle volume fraction, where a linear relationship is observed. The increase in yield strength values in comparison with the particle-free deposits is of the same order of magnitude as previously reported results [18]. The stronger hardening effect of smaller particles is in agreement

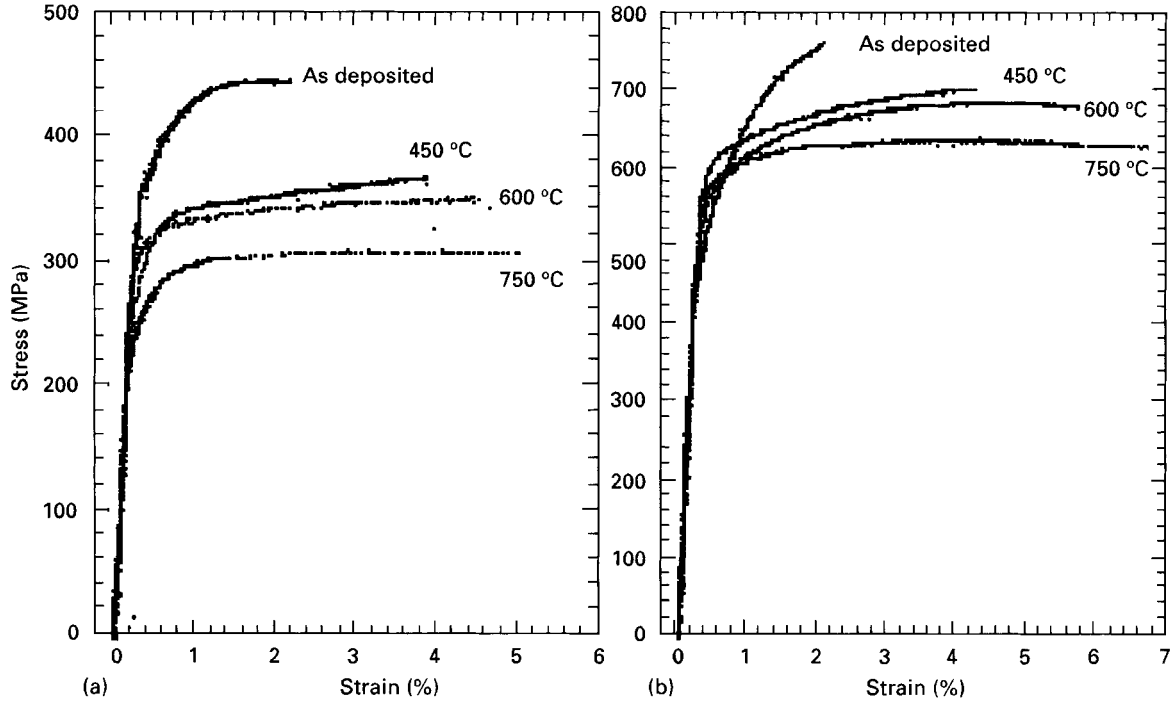

Figure 4 Stress–strain curves of (a) Cu–8%AOM and (b) Ni–9%AOM deposits.

TABLE III Mechanical properties of Cu–8%AOM and Ni–9%AOM deposits

Annealing temperature (°C)	0.2% yield stress (MPa)		Ultimate stress (MPa)		Elongation (%)	
	Cu–AOM	Ni–AOM	Cu–AOM	Ni–AOM	Cu–AOM	Ni–AOM
As deposited	242	370	446	765	3.6	2.8
450	228	346	378	712	4.8	4.1
600	209	324	338	688	6.1	5.3
750	199	302	306	665	6.7	5.8

with the microhardness results. By plotting the hardening slope of each set of specimens against the particle size, as in Fig. 5b, the size dependence of particle strengthening is revealed. Indeed, the strengthening effect is stronger in the submicron range of particle size while, for the particles of size more than 1 μm, the strengthening is not only much reduced, but also less sensitive to the particle size.

The ductility of the as-deposited composites is presented in Fig. 6 in terms of elongation obtained from tensile tests. Table IV gives the ductility data of annealed deposits. As expected, the particle-reinforced deposits are much more brittle than the pure metal deposits, and this embrittlement increases with decreasing particle size. The deposits containing alumina of 0.11 μm average size are the most brittle with a strain value not exceeding 3.5%. The same order of elongation (2%) has been previously observed in the case of Ni–2.4%Al_2O_3 deposits with particle size less than 0.3 μm [15]. After heat treatment, a general improvement in ductility is observed except for the Cu–AOS deposits.

4. Discussion

The observed linear increase in microhardness and strength of composite deposits with increasing particle volume fraction has been previously reported [13–16, 18]. It was further shown that submicron particles have a stronger hardening effect and a better hardness and yield strength retention after annealing. By comparing the obtained values, the hardness-to-yield-strength ratio is between 5 and 7. This ratio is somewhat between the value of 3 corresponding to a fully strain hardened metal and the value of 9.5 for a fully annealed (relaxed) metal [22, 23]. This indicates that the deposits studied are between the two extreme states.

Microstructural investigation shows that, upon annealing, the grains of particle-free deposits undergo a rapid growth while the grains of composite samples grow more slowly, owing to the "pinning" effect of particles on the grain boundaries [8, 19]. For example, after annealing for 1 h at 750 °C, the grains of Cu–8% AOM deposits at best doubled, while the size of grains of pure copper foils grew by almost 20 times. The good retention in microhardness and strength exhibited by annealed composite samples is attributed to the restrained grain growth of these deposits.

Since the composite deposits are produced at temperatures usually below 50 °C, there is neither interfacial diffusion nor internal stress due to the thermal expansion coefficient difference of the two phases. Locally, under stress, particles act as plastic strain

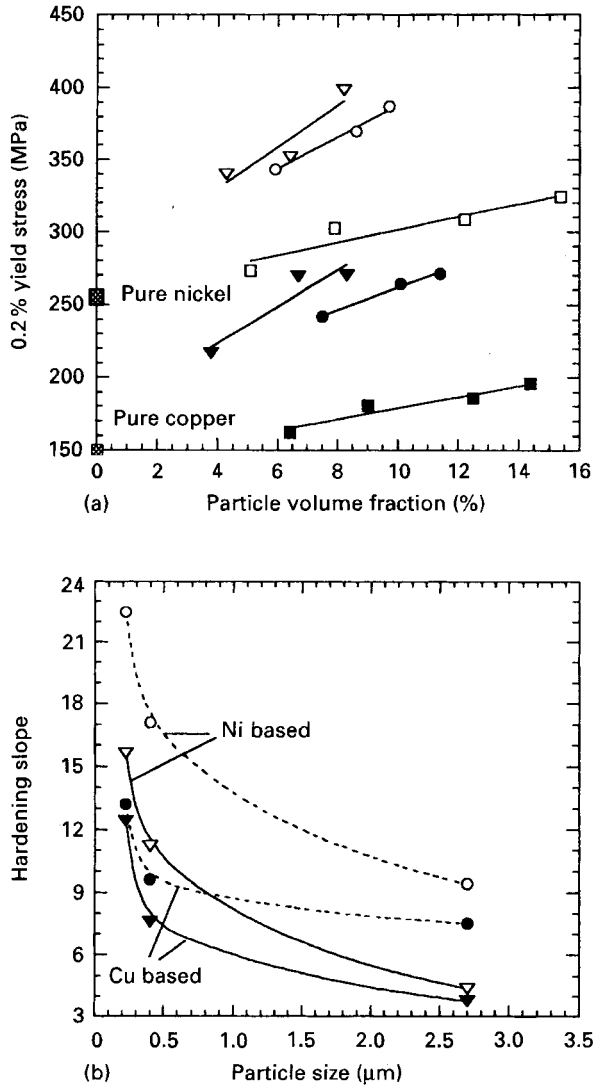

Figure 5 (a) 0.2% yield stress of metal–alumina deposits as a function of particle volume fraction ((▽), Ni–AOS; (○), Ni AOM; (□), Ni-AOL; (▼), Cu–AOS; (●), Cu–AOM; (■), Cu–AOL) and (b) variation in hardening slope with particle size ((—), strength; (- - - -), hardness).

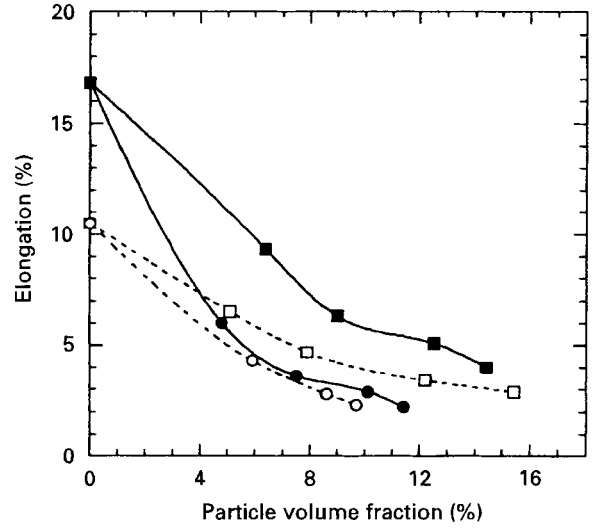

Figure 6 Elongation of as-deposited metal–alumina specimens versus particle volume fraction ((■), Cu–AOL; (●), Cu–AOM; (□), Ni–AOL; (○), Ni–AOM).

TABLE IV Elongations of annealed pure metal and metal–alumina deposits where the particle volume fractions are the same as in Fig. 2

Matrix	Particles	Elongation (%) for the following annealing temperatures			
		25 °C	450 °C	600 °C	750 °C
Copper	None	16.8	20.1	23.7	30.2
	AOL	4.1	6.7	7.8	9.4
	AOM	3.6	4.8	6.1	6.7
	AOS	3.1	3.5	2.8	2.6
Nickel	None	10.5	14.1	19.2	32.0
	AOL	2.9	4.6	6.7	12.7
	AOM	2.8	4.1	5.3	5.8
	AOS	1.0	1.2	1.6	2.0

incompatibilities within the ductile matrix, hindering dislocations from moving further in their slip planes. A transmission electron micrograph showing particles which act as barriers to dislocation movement is presented in Fig. 7 for an as-deposited Ni–9%AOM sample after a tensile test. The strengthening resulting from the dispersed particles depends on the distribution features of particles, namely, the average particle size, ϕ_p, and mean interparticle distance, λ. Since the incorporated particles are fully incoherent with the matrix, Orowan strengthening can be reasonably proposed, at least for finer particles. The critical shear stress for yielding of a composite deposit follows the simple relationship

$$\tau_c = \tau_m + \frac{Gb}{\lambda - \phi_p} \quad (1)$$

where τ_c and τ_m are the critical shear stresses of the composite and of the matrix, respectively, G is the shear modulus of matrix material and b is the Burgers vector.

The calculated yield strengths of as-deposited metal-alumina samples are presented in Fig. 8, together with the experimentally measured values. As can be seen, the experimental results show a higher strengthening than the theoretical prediction from the Orowan mechanism. Thus, although particles are efficient obstacles to the movement of dislocations, there must be additional microstructural features which play a role in the strengthening of the composite deposits. It was previously reported that particles act as new sites for nucleation during deposition, leading to the creation of large-angle grain boundaries and a refinement of matrix grains [8, 19]. Furthermore, the codeposited particles hinder the matrix grain growth during heat treatment. Thus a mechanism based on grain-boundary strengthening should also contribute to the hardening of composite deposits. The grain-boundary strengthening was estimated using the Hall–Petch relation

$$\sigma_y = \sigma_i + k\phi_m^{-1/2} \quad (2)$$

where σ_y and σ_i are the yield strength and the frictional stress, respectively, k is a constant and ϕ_m is the average matrix grain size.

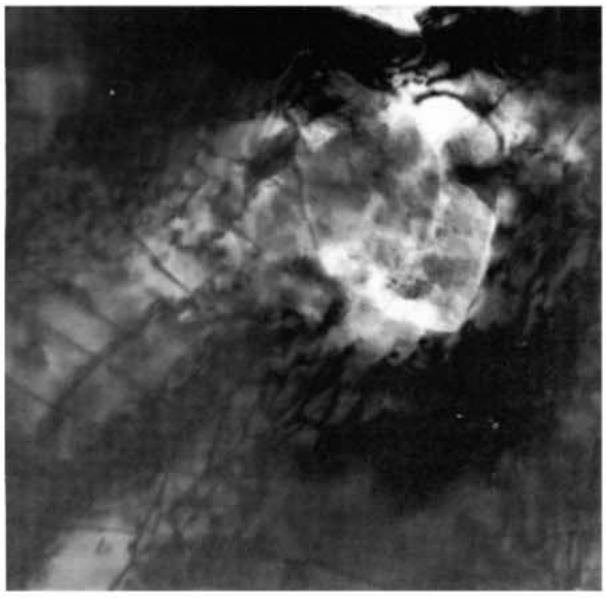

Figure 7 Transmission electron micrograph of an as-deposited Ni–9%AOM sample after a tensile test, showing that dislocations were hindered at a matrix–particle interface.

The experimentally obtained yield stress and microhardness values of annealed pure metal and metal–alumina deposits are plotted in Fig. 9 versus the reciprocal square root of the grain size, ϕ_m. A fairly good fit of the linear relation for each group of specimens is noted. For the same base metal, the lines corresponding to the composite samples are nearly parallel to those of pure metal samples, e.g. composite and metal samples have very similar k values, but the composite samples show a higher strength and hardness than do the pure metal deposits. The difference in strength is around 30–50 MPa. This is in fact very close to the stress increments calculated by Equation 1 (see Fig. 8). The σ_i and k values for the pure Ni and the Ni–AOM deposits obtained from Fig. 9 are listed in Table V together with the those reported by Thompson [24] for pure nickel. The k values of our system are close to the reported value. The higher σ_i in our case may have resulted from the finer grain size.

The question of how important the relative contribution of either hardening mechanism is in the

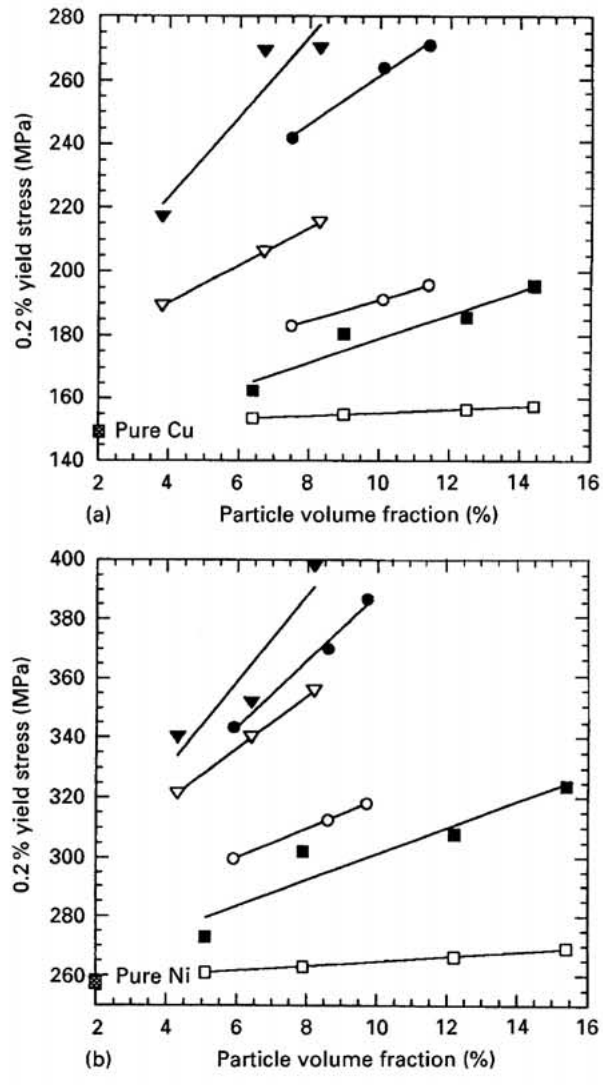

Figure 8 Calculated (▼, ●, ■) and experimentally measured (▽, ○, □) yield stresses of (a) copper–alumina ((▽), (▼), Cu–AOS; (○), (●), Cu–AOM; (□), (■), Cu–AOL) and (b) nickel–alumina deposits ((▽), (▼), Ni–AOS; (○), (●), Ni–AOM; (□), (■), Ni–AOL), as functions of particle volume fraction.

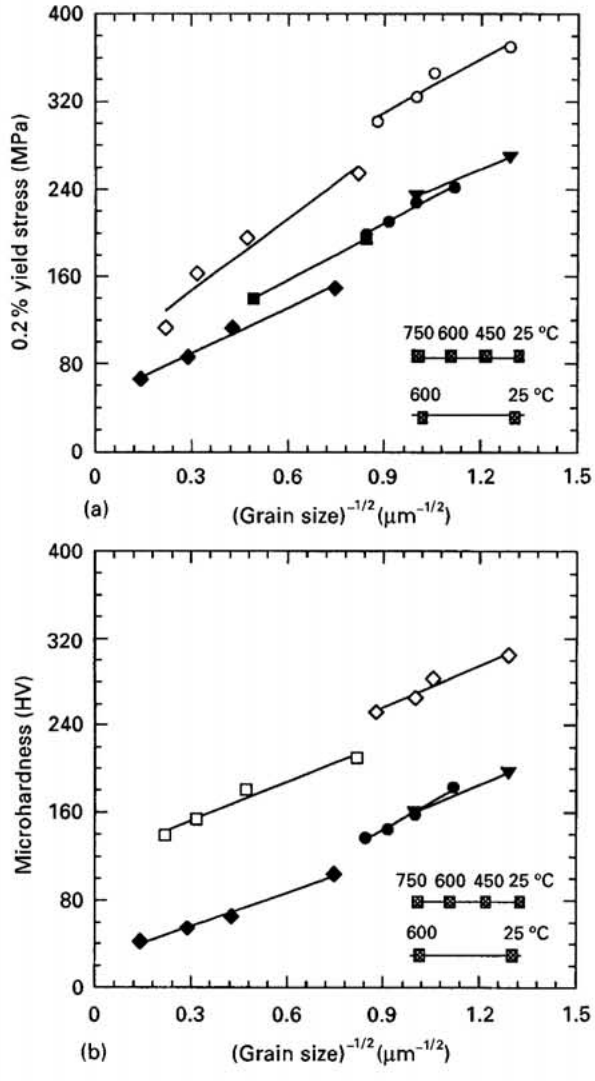

Figure 9 Variation in (a) 0.2% yield stress ((◆), pure Cu; (▼), Cu–AOS; (●), Cu–AOM; (■), Cu–AOL; (◇), pure Ni; (○), Ni–AOM) and (b) microhardness with reciprocal square root of matrix grain size ((◆), pure Cu; (▼), Cu–AOS; (●), Cu–AOM; (□), pure Ni; (◇), Ni–AOM). The schematic insets indicate the corresponding annealing temperatures.

TABLE V σ_i and k values

Specimen	σ_i (MPa)	k (MN m$^{-3/2}$)
Pure Ni	80.2	0.22
Ni–AOM	154.5	0.17
Massive Ni [24]	21.8	0.16

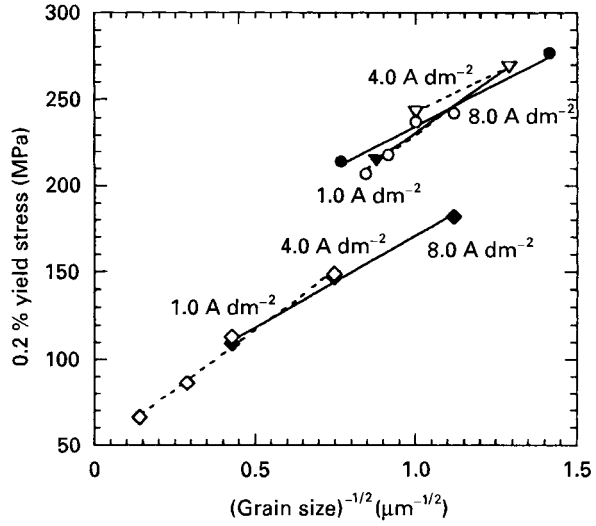

Figure 10 Relationship between 0.2% yield stress and reciprocal square root of grain size of as-deposited (—, ◆, ▼, ●) and annealed (- - -, ◇, ▽, ○) coatings ((◆), (◇), pure Cu; (▼), (▽), Cu AOS; (○), (●), Cu–AOM). The corresponding deposition current densities for as-deposited samples are also indicated.

as-deposited state is not clear from the above discussion. Indeed, bearing in mind that as-deposited composites have a smaller matrix grain size, Hall–Petch hardening might also govern the as-deposited states. In this case, a pure matrix deposit, produced at a higher current density with a smaller grain size, should show about the same increase in the yield stress as a composite deposit with a similar grain size. This is not the case since, as presented in Fig. 10, the yield stress values of as-deposited copper–alumina deposits are definitely higher (around 60 MPa) than those of the particle-free deposits having the same grain size. Again, the difference between the two stresses is close to the stress increment calculated from Equation 1. This analysis leads to the conclusion that both dispersion and grain-boundary hardening are effective in the as-deposited state. Furthermore, by superimposing the data obtained from heat-treated samples, this same figure (see Fig. 10) shows more clearly the dispersion-hardening contribution after annealing. The slightly higher dispersion-hardening values in the annealed case is, in our opinion, a reflection of the interfacial strength: upon annealing, the bonding strength of the interfaces either is kept at the same level or is slightly increased. Finally, it should be emphasized that a higher matrix defect density in the composite specimens [8] would also contribute to the observed strengthening.

5. Conclusion

Composite coatings with different volume fractions of alumina powders were produced using electroplating showing much higher strength and hardness than particle-free deposits do. The hardening mechanism of composite coatings was shown to be a combined effect of both dispersion hardening and grain-boundary hardening. The contribution of each effect has been separated and quantitatively measured.

Acknowledgements

This work has been performed under the auspices of the Swiss National Funds for Scientific Research Contract 21. 037. 439.

References

1. V. P. GRECO, *Plat. Surf. Finish.* **76** (1989) 68.
2. *Idem., ibid.* **76** (1989) 62.
3. C. A. ADDISON and E. C. KEDWARD, *Trans. Inst. Metal Finishing* **55** (1977) 41.
4. A. WASSERMAN, *Met. Finish.* **87** (1989) 47.
5. M. THOMA, *Plat. Surf. Finish.* **71** (1984) 30.
6. J. FOSTER and B. CAMERON, *Trans. Inst. Met. Finish.* **54** (1976) 178.
7. C. WHITE and J. FOSTER, *ibid.* **59** (1981) 8.
8. X. M. DING, PhD thesis 1117, Swiss Federal Institute of Technology, Lausanne (1993).
9. E. C. KEDWARD, K. W. WRIGHT and A. A. B. TENNETT, *Tribol. Int.* No. 10 (1974) 221.
10. X. M. DING, N. MERK and B. ILSCHNER, in "Proceedings of the Third International Conference on Functionally Gradient Materials", Lausanne, October 1994, edited by B. Ilschner and N. Cherradi (Presses Polytechniques et Universitaires Romanes, Lausanne, 1995) p. 365.
11. J. ZAHAVI and J. HAZAN, *Plat. Surf. Finish.* **70** (1983) 57.
12. E. C. KEDWARD and K. W. WRIGHT, *ibid.* **65** (1978) 38.
13. A. RAMASAMY and M. TOTLANI, *J. Electrochem. Soc. India* **76** (1977) 25.
14. G. R. LAKSHMINARAYANAN, E. S. CHEN and F. K. SAUTTER, *Plat. Surf. Finish.* **63** (1976) 35.
15. V. P. GRECO and W. BALDAUF, *Plating* **55** (1968) 250.
16. F. K. SAUTTER, *J. Electrochem. Soc.* **110** (1963) 557.
17. G. E. DIETER, "Mechanical metallurgy" (McGraw-Hill, London, 1988).
18. V. M. VERELST, J. P. BONINO and A. ROUSSET, *Mater. Sci. Eng.* **A135** (1991) 51.
19. N. MERK, X. M. DING and B. ILSCHNER, *J. Mater. Sci.* submitted.
20. R. RAMASWAMY, *Met. Finish.* No. 9 (1992) 23.
21. "Metals handbook" (American Society for Metals, Metals Park, OH, 10th Edn, 1990).
22. M. PUSHPAVANAM, *Met. Finish.* No. 10 (1974) 46.
23. J. B. CAHOON, W. H. BROUGHTONAND and A. R. KUTZAK, *Metall. Trans.* **2** (1986) 93.
24. A. W. THOMPSON, *Acta Metall.* **25** (1977) 83.

Received 15 May 1996
and accepted 20 January 1997